Finite Element Studies of the Electro Impulse De-Icing System

R. J. Scavuzzo* and M. L. Chu*
University of Akron, Akron, Ohio 44325
E. J. Woods†
Boeing Commercial Airplane Company, Seattle, Washington
R. Raju‡
University of Akron, Akron, Ohio 44325
and
A. A. Khatkhate§
Innovative Dynamics, Ithaca, New York

In this study, analytically determined impulsive forces of an electro impulse de-icing (EIDI) system are used as input to a finite element model to predict the dynamic response of an airfoil coated with impact ice. By making use of the basic mechanical properties of impact ice and the test results on the EIDI system, a comparison is made between finite element calculations and measured displacements on an airfoil section. Experimental data were provided in the form of time-dependent displacements along both the transverse and lateral directions of the leading edge of an airfoil section. A finite element model of the EIDI system using MSC Nastran was developed with plate elements representing the aluminum skin of the test section and the accreted impact ice. Weightless stiff beam elements provided the shear connection between the ice and aluminum elements. Force-time history was input through eight nodes at the coil location.

Nomenclature

a = radius of the current carrying loop, m
E_{loop} = external voltage applied to the loop
I_{loop} = loop current, A
R = loop resistance, Ω
r = radius at which A_Φ is evaluated, m
t = time, s
z = axial distance at which A_Φ is evaluated, m
μ_0 = $4\pi \times 10^{-7}$, weber/A-m
Φ = total flux linking the loop, weber

Introduction

PATENTS on de-icing by an electric impulse de-icing system (EIDI) system were first obtained in 1930. An aircraft equipped with an EIDI system has operated in the USSR since 1972. At that time, several firms in England and the US studied and tested EIDI systems but then dropped them. More recently, Zumwalt[1-3] and his colleagues at Wichita State University have completed extensive studies and development of the system and have installed it on aircraft.

In this study, an approximate finite element model of an airfoil section fitted with an EIDI system was developed to compare measured deflections with calculated values and to predict the ice shedding area with finite element analysis and to compare these analytical results with measured values. In order to meet these objectives, the finite element analysis must accurately model the metal-ice composite stiffness and inertia. Also interface stresses between the ice and airfoil surface must be determined from the model if ice shedding is to be evaluated.

Presented as Paper 88-0022 at the AIAA 26th Aerospace Sciences Meeting, Reno, NV, Jan. 11-14, 1988; received Sept. 15, 1988; revision received Feb. 12, 1990.

*Professor, Department of Mechanical Engineering.
†Principal Engineer.
‡Graduate Student, Department of Mechanical Engineering.
§Engineer.

The airfoil surface and ice was modeled as two layers of plate elements representing the aluminum skin and the impact ice layer, respectively. Weightless, stiff beam elements were used to connect the two layers of plate elements and to obtain the shear stresses at the aluminum-ice interface. Shear between the two plates is carried by the beam elements. Shear stresses are determined by the shear force in the beams and one quarter of the area of four adjacent elements.

An attempt was made to use a composite finite element of two layers to model the structure with one layer representing the metal airfoil skin and the other layer the impact ice. This modeling could be used to obtain static bending stresses in the two layers and shear stresses at the interface. However, dynamic effects were not represented accurately. It appears that the inertia of both layers are lumped in one plane and, therefore, the resulting dynamic stresses in the composite could not be accurately calculated. For this reason, the approximate model just described was developed.

In a previous study, the displacement-time history at the center of the coil location was prescribed as input to the airfoil section through a seismic mass.[4] A direct transient solution was used to calculate displacements, stresses, and forces in the model. A good correlation was established between the shedding of ice predicted by this approximate analytical method and experimental observations.

In this paper, the structural model of the airfoil test section fitted with an EIDI system described in Ref. 4 is excited by an analytically determined force-time history input rather than the measured displacement-time history input previously used. The essential constituents of this analytical model are described, including the analysis of the EIDI impulse and force inputs to the airfoil section. Displacement-time histories of the bending waves developed by the EIDI coil were measured along both the transverse and lateral directions. Properties of impact ice in this model are taken from Refs. 1 and 2. Calculated displacements are compared to experimental measurement.

Force-Time History

Boeing Commercial Airplane Company conducted a series of tests on an airfoil having a cross section for the 7J7 airplane. This airfoil is shown in Fig. 1 and in cross section along

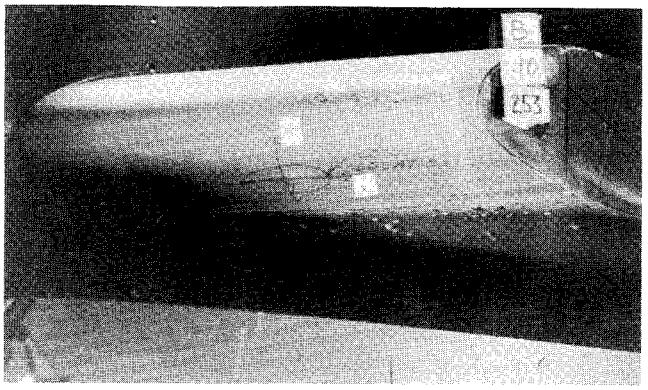

Fig. 1 Electric coil location on the airfoil section before de-icing.

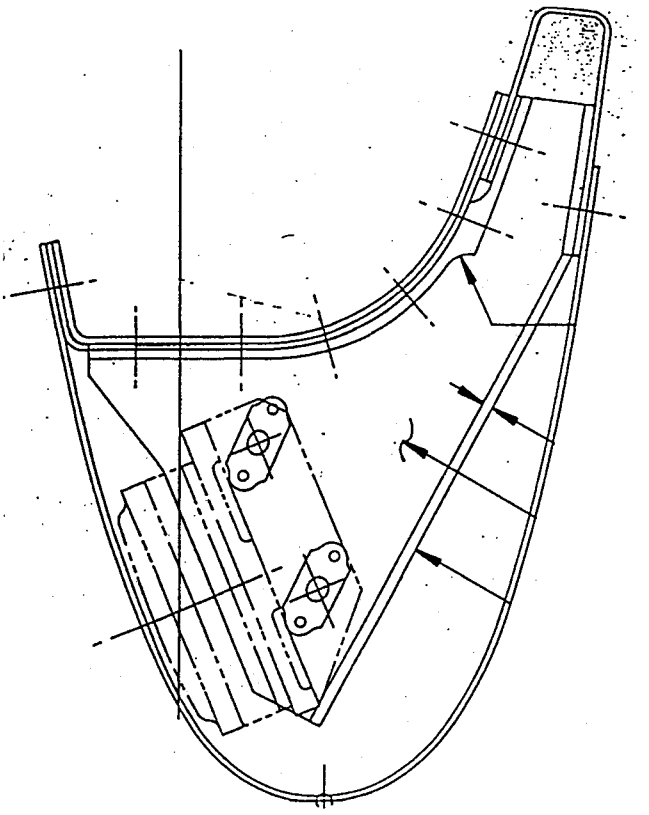

Fig. 2 Airfoil cross section showing coil location.

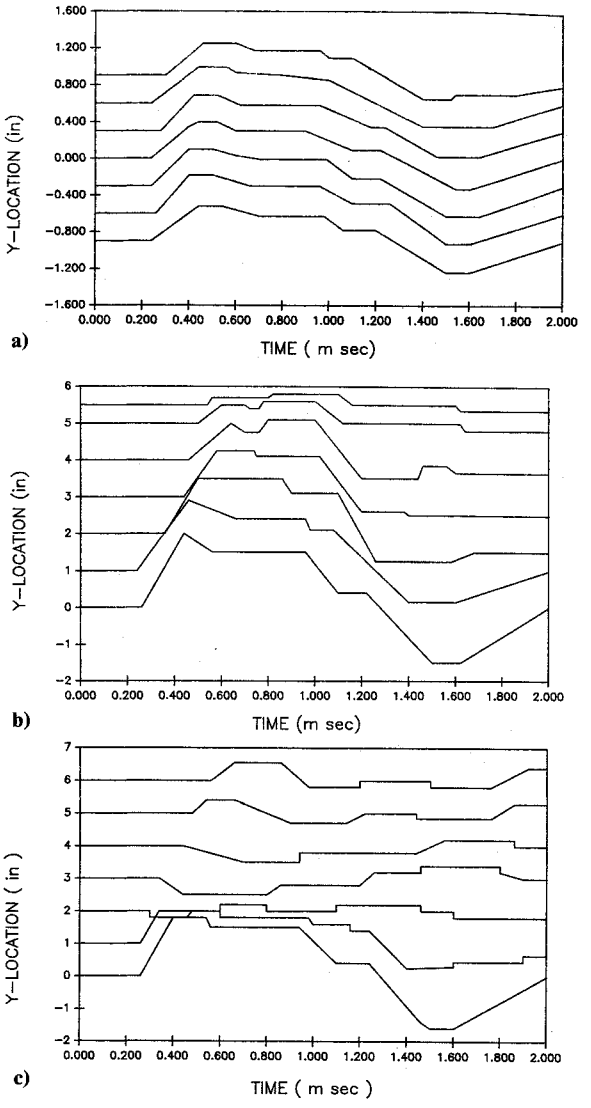

Fig. 3 Typical displacement-time history measured with holography. The coordinate directions are shown in Figs. 1 and 10. Displacement magnitude is equal to *Y*-axis location divided by 10 on Fig. 3a, and divided by 50 on Figs. 3b and 3c.

with the coil location in Fig. 2. The tests were conducted with a coil having 25 turns. The maximum deflection occurred near the coil center. Displacement, as a function of time, was measured using holographic methods along both the transverse and lateral directions around this location as shown in Figs. 3a–3c. The apparent step response of the measured surface is associated with the holographic measurement techniques. Calculations of the coil current, the skin pressure vs time and radius, and the impulse vs time based on the peak current of 1650 A and a rise time of 13 μs are shown in Figs. 4–7, respectively. The calculation of skin pressure vs time was performed at Boeing using a FORTRAN language computer simulation program written for this project. The program accepted coil dimensions as input along with information on skin conductivity, skin thickness, capacitor value, and charge voltage.

The skin is assumed to be flat circular plate. In turn, the plate is assumed to be a current-carrying conductor loop, and the aluminum skin is subdivided into about 30 circular loops. Each current-carrying loop produces magnetic flux that links all other loops. At each time step of the solution, the differential equations of all current loops are solved simultaneously. The form of the differential equation is

$$E_{\text{loop}} = R \times I_{\text{loop}} + \frac{d\Phi}{dt} \tag{1}$$

For numerical evaluation, $d\Phi$ becomes $\delta\Phi$, the change in flux linking the loop during a time step of δt, and I_{loop} becomes the average current during the time step.

Several constraints are imposed on the solution as follows:

1) All coil loops carry the same current.

2) The sum of all coil loop voltages is equal to the voltage applied by the capacitor bank as it discharges minus the voltage drop across any series impedance.

3) Each aluminum skin loop is a short circuit and has zero volts applied.

4) During each time step, the capacitor voltage is constant and updated only at the end of each time step.

The calculation of flux linking each current loop is a function of the current in all loops and can be calculated by summing the flux contribution from all loops. The individual loop contribution can be obtained by evaluating the magnetic vector potential from Eq. (2).[5]

$$A_\Phi = \int_0^{\pi/2} \frac{\mu_0 a I_{\text{loop}} (2\sin^2\Theta - 1)\, d\Theta}{\pi\left[(a+r)^2 + z^2 - 4ar\sin^2\Theta\right]^{1/2}} \quad (2)$$

The integral equation [Eq. (2)] is numerically evaluated, and flux density and total flux for any loop is obtained by summing over all loops and then differentiating with respect to radius and axial distance. The solution of the differential equations resulted in a coil current, which is shown in Fig. 4.

From the value of flux density and loop currents, forces on any loop can be calculated. In particular, the forces on current skin loops can be obtained and divided by loop area to give the values of pressure shown in Figs. 5 and 6. If the total force on the aluminum skin is multiplied by the time increment and summed for the total time period of interest, then impulse, as shown in Fig. 7, is obtained. The calculated final value of the impulse shown in Fig. 7 compared very well (less than 5% error) with Boeing laboratory data using an EIDI coil on a ballistic pendulum. The calculated values of impulse also agreed quite well for other materials such as titanium and stainless steel, which were tested during this project. Nodal force history is shown in Fig. 8.

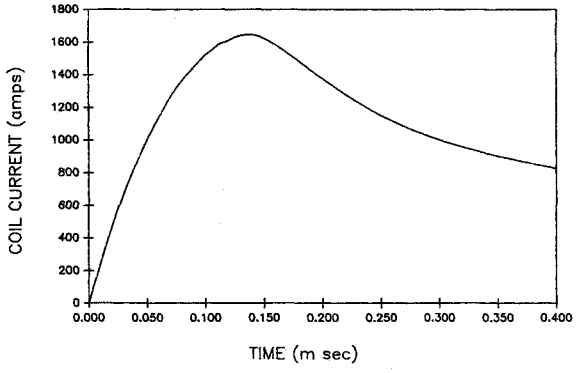

Fig. 4 Coil current transient.

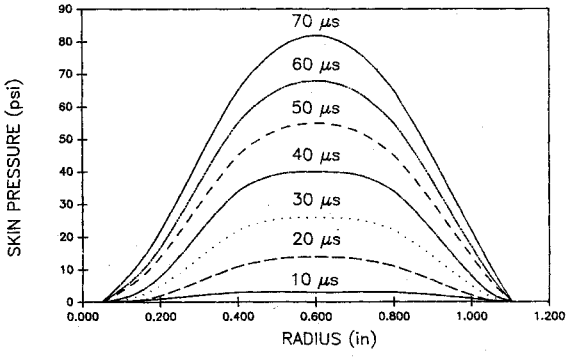

Fig. 5 Skin pressure transient from 0 to 70 μs.

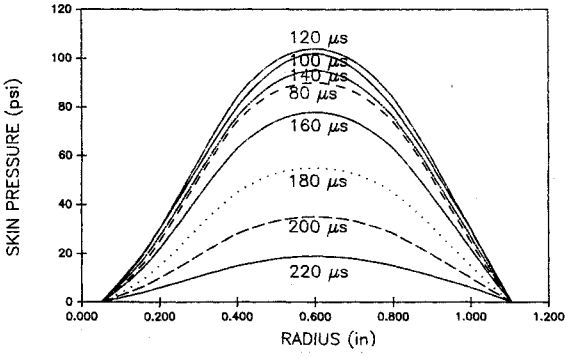

Fig. 6 Skin pressure transient from 80 to 220 μs.

Approximate Finite Element Model

In this approximate model, as in Ref. 7, four noded plate (CQUAD4) elements were used to describe the aluminum skin and the outer accreted ice layer as shown in Fig. 9. These elements are made finer at the leading edge where the curvature is higher. The inner layer of 3952 CQUAD4 elements representing the aluminum skin have the geometric and physical parameters that are summarized in Table 1. Properties of the outer layer of 3952 CQUAD4 elements representing the accreted ice layer are also listed in Table 1.

Weightless, short, stiff beam elements (CBAR) that are 0.156 in. long provide the shear connection between the ice and aluminum elements. Properties of beam elements are listed in Table 2.

Both the CQUAD4 elements and the CBAR elements are assumed to have materials with linear, temperature-independent isotropic properties.

On the results reported in this model, there are 8162 grid points. A rectangular coordinate system with origin at the grid point 3117, which is approximately the location of the center

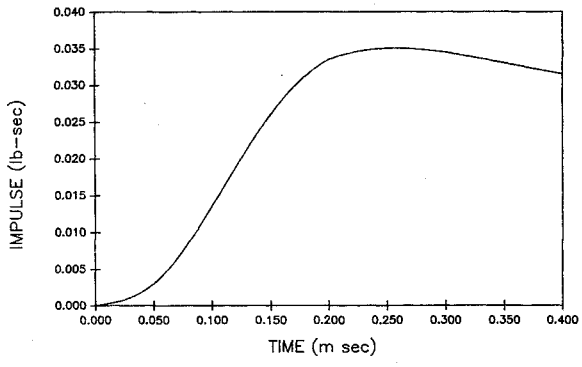

Fig. 7 Skin impulsive transient from 0 to 400 μs.

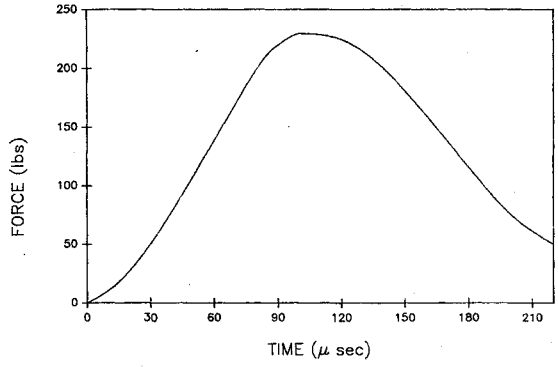

Fig. 8 Skin force transient from 0 to 240 μs.

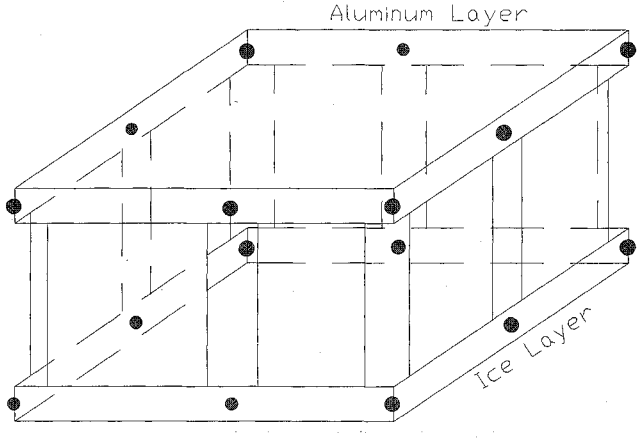

Fig. 9 Approximate finite element modeling approach.

Table 1 Finite element properties

	Plate properties	
	Aluminum skin	Accreted ice
Plate thickness, in.	0.1	0.25
Young's modulus, psi	10×10^6	0.8×10^6
Poisson's modulus, psi	0.3	0.3
Density, lb-s^2/in.^{4}	2.59×10^{-4}	0.842×10^{-4}

Table 2 Beam properties

Area, in.^{2}	1000
$I_x = I_y$, in.^{4}	100
E, psi	10^{10}
Poisson's ratio	0.3
J, in.^{4}	200

Table 3 Grid point coordinates, in.

Grid point	X	Y	Z
3117	0.0000	0.0000	0.0000
2347	0.0000	−0.5000	−1.0200
1192	0.0000	−2.2900	−0.8000
807	0.0000	−3.1700	0.2200
422	0.0000	−3.8500	1.3900
3108	−1.9575	0.0000	0.0000
3099	−3.9150	0.0000	0.0000
3089	−6.0900	0.0000	0.0000

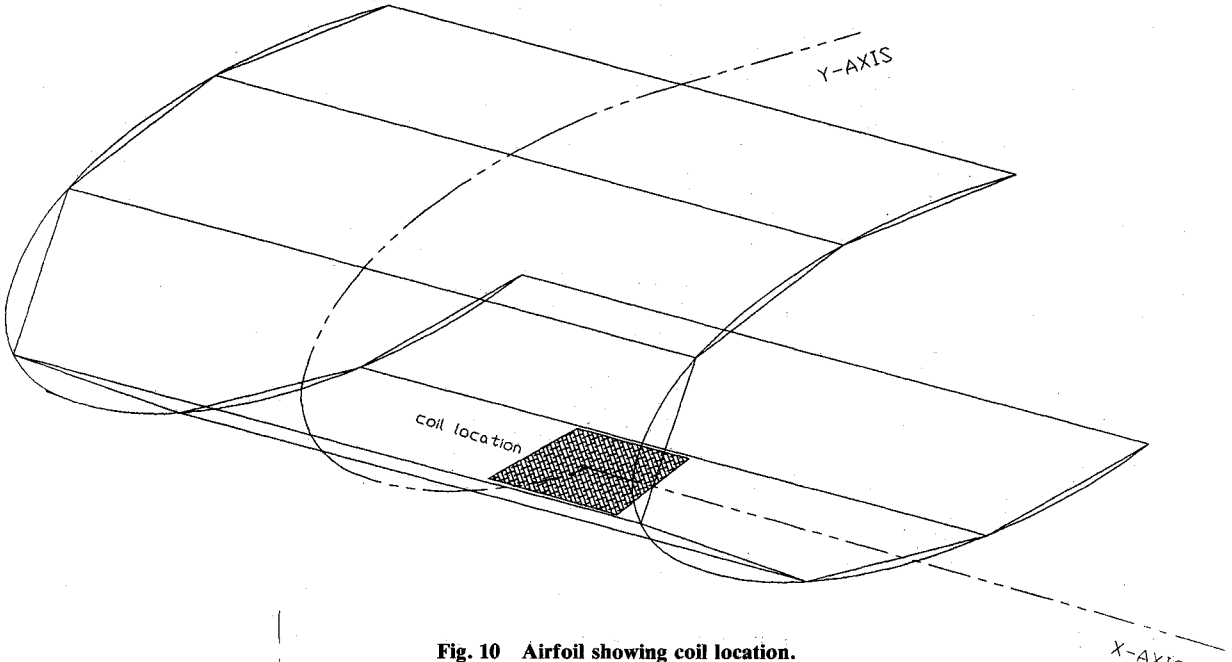

Fig. 10 Airfoil showing coil location.

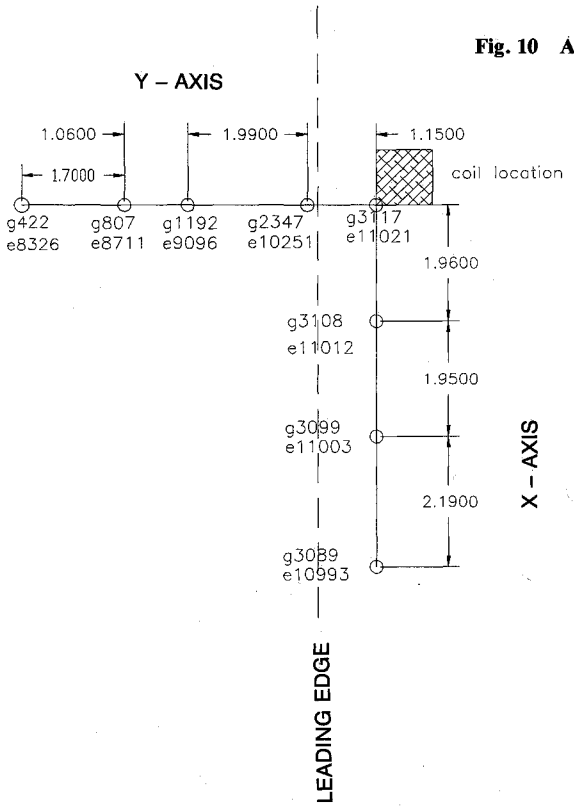

Fig. 11 Position of nodes and elements on the airfoil.

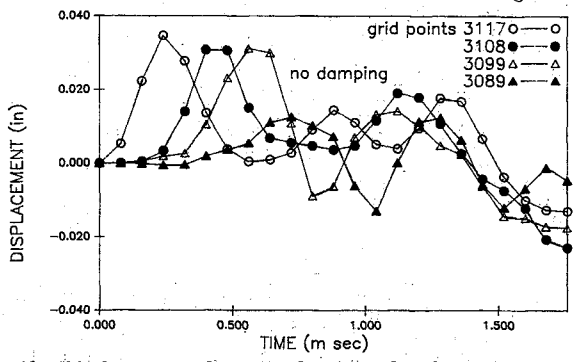

Fig. 12 Displacement along the leading edge from the coil (grid 3117) to 6 in. from the coil (grid 3089) with no damping.

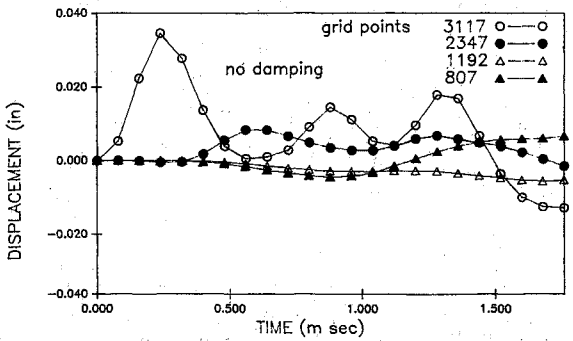

Fig. 13 Displacement along the chord from the coil (grid 3177) to 4 in. from the coil (grid 807) with no damping.

Table 4 Comparison of measured and calculated deflections along the leading edge

Grid point	Distance from coil, in.	Calculated deflection, in. 0% damping value	5% damping value	10% damping value	Measured deflection
3117	0.0000	0.035	0.035	0.030	0.040
3108	1.9575	0.032	0.033	0.023	0.030
3099	3.9150	0.032	0.033	0.021	0.020
3089	6.1000	0.011	0.010	0.009	0.008[a]

[a]Measured value at 5.5 in. from coil.

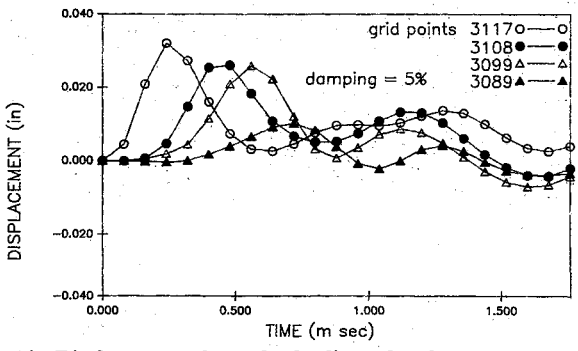

Fig. 14 Displacement along the leading edge from the coil (grid 3117) to 6 in. from the coil (grid 3089) with 5% damping.

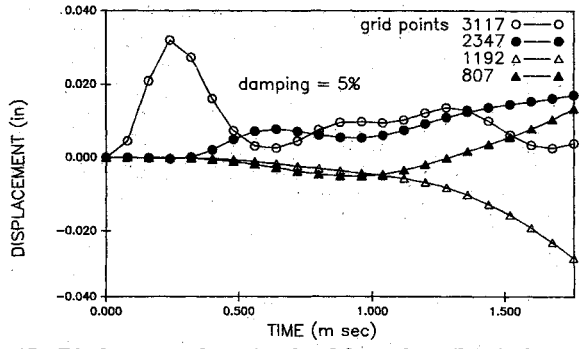

Fig. 15 Displacement along the chord from the coil (grid 3117) to 4 in. from the coil (grid 807) with 5% damping.

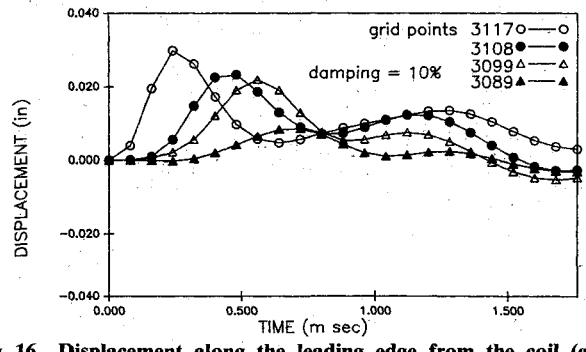

Fig. 16 Displacement along the leading edge from the coil (grid 3117) to 6 in. from the coil (grid 3089) with 10% damping.

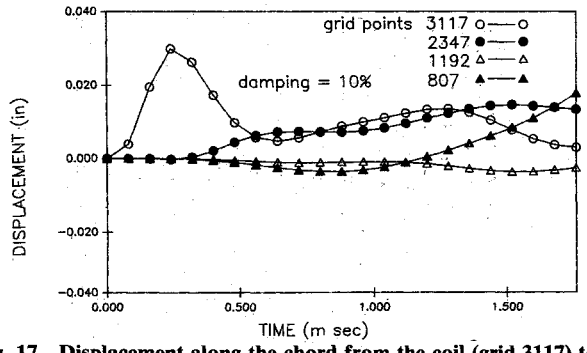

Fig. 17 Displacement along the chord from the coil (grid 3117) to 4 in. from the coil (grid 807) with 10% damping.

Table 5 Comparison of measured and calculated deflections along the chord

Grid point	Distance from coil, in.	Calculated deflection, in.[a] 0% damping value	5% damping value	10% damping value	Measured deflection
3117	0.0000	0.035	0.035	0.030	0.040
2347	1.1500	0.020	0.008	0.008	0.020
1962	3.1400	0.090	−0.040	0.000	−0.010
807	4.2000	0.090	−0.003	−0.002	−0.020

[a]Peak deflection 0 to 1 ms.

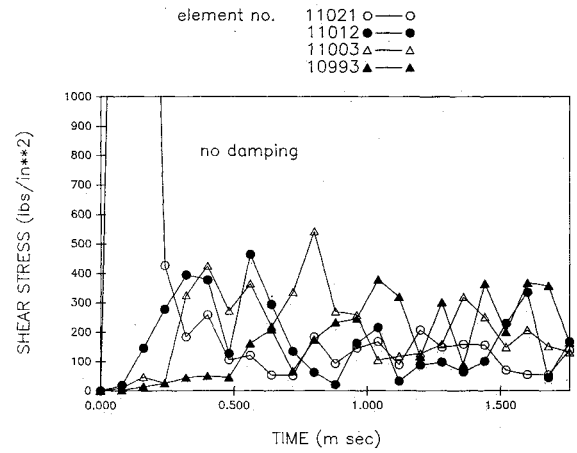

Fig. 18 Shear stress in bar elements along the leading edge from the coil (element 11021) to 6 in. from the coil (element 10993) with no damping.

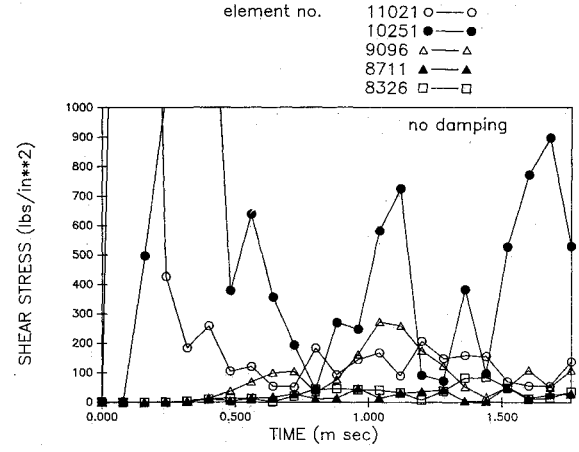

Fig. 19 Shear stress in bar elements along the chord from the coil (element 11021) to 6 in. from the coil (element 8326) with no damping.

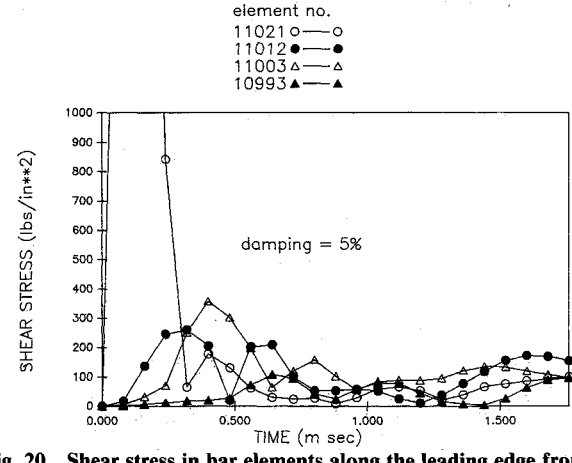

Fig. 20 Shear stress in bar elements along the leading edge from the coil (element 11021) to 6 in. from the coil (element 10993) with 5% damping.

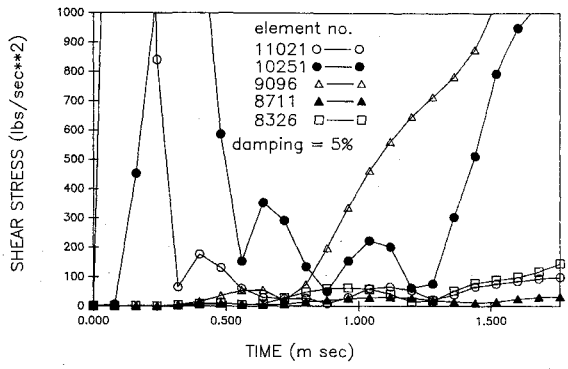

Fig. 21 Shear stress in bar elements along the chord from the coil (element 11021) to 6 in. from the coil (element 8326) with 5% damping.

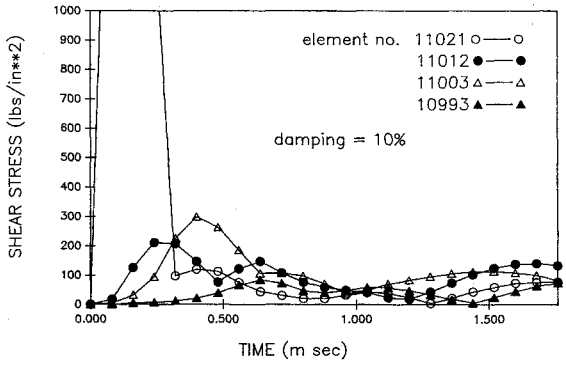

Fig. 22 Shear stress in bar elements along the leading edge from the coil (element 11021) to 6 in. from the coil (element 10993) with 10% damping.

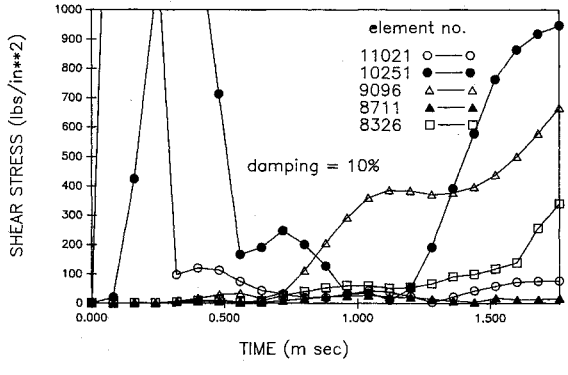

Fig. 23 Shear stress in bar elements along the chord edge from the coil (element 11021) to 6 in. from the coil (element 8326) with 10% damping.

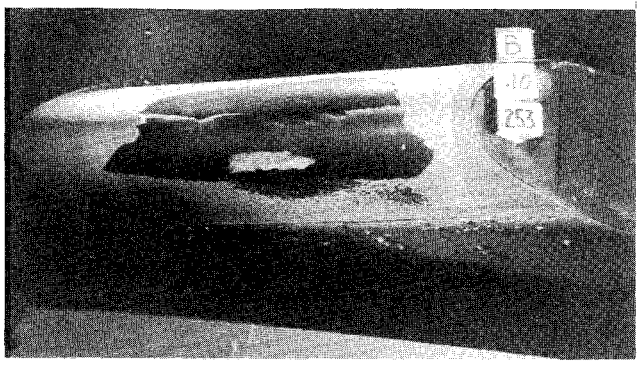

Fig. 24 Airfoil showing region of ice shedding.

of the coil, is used. The node points at the edges of the airfoil are constrained in all the six directions. All other node points are constrained in all rotational directions. Without this constraint, convergence could not be obtained. Grid points used in the output are listed in Table 3.

The position of the coil is shown in Figs. 10 and 11. A grid point 9045, with all six independent degrees of freedom assigned to it, is defined at some distance away from the coil position. A rigid body element (RBE2) connects this grid point to all eight grid points of the coil location. An eighth of the effective force-time history calculated earlier, as in Fig. 8, is imposed on each of the eight nodes, as shown in Fig. 10. The calculated displacement-time history was compared with the desired displacement-time motion. The damping was introduced using 2 PARAM cards in the NASTRAN program inputs. Since the displacement-time history has a frequency of 1000 Hz, the damping ratio was specified at this frequency. Different damping ratios were tried. The best correlation between the desired displacement-time motion and calculated displacement-time history and stress response was obtained with 5% damping (Figs. 12 and 13).

The displacement at point 3117 in the layer of CQUAD4 elements representing the aluminum skin and the shear forces in the BAR elements are obtained using a direct transient solution.

Shear forces in the BAR elements are studied and are used to calculate the shear forces at the interface. One quarter of the area of all the four elements is used to determine the interface shear stress from the beam shear force. Time history plots of shear stresses in the upper left quadrant of the airfoil along the chord and axial directions at specific grids are calculated. Failure is assumed to occur if this stress reaches 50 psi.

Various values of viscous damping were specified with the objective of accounting for the energy dissipation associated with ice shedding. In this study, results from damping values of 0, 5, and 10% were examined.

Results

As seen in Fig. 3, the measured peak displacement is 0.040 ± 0.10 in. Calculated peak values are 0.035, 0.0034, and 0.030 in. for damping values of 0, 5, and 10%, respectively. Readings at times after 1 ms are too great for the 0% damping. A value of 5% gives the best correlation with data. At the coil grid point (3117), the maximum deflection from the measured data seems to dwell longer than the analytical solution. Deflections are presented along the leading edge on grid points 3108, 3099, and 3089, which are spaced at 2-in. intervals from the core location of grid point 3117. Peak calculated values are compared to those measured in Table 4. Agreement is reasonable.

Calculated deflections along the chord direction (Figs. 12–17) decrease much more rapidly as the bending wave travels around the leading edge. This trend also can be observed in the measurements shown in Fig. 3c. Furthermore, initial deflections at some grid points are in the negative (inward) deflection of the airfoil. This trend is also observed in the measurements. After about 1 ms, deflections at some grid points began to increase in a divergent manner, which indicated numerical instability in the NASTRAN calculations. Because of the rapid loading, time steps of 1 μs were specified, which leads to significant instability in the calculation after 2 ms.

Shear stresses are plotted in Figs. 18–23. Ice shedding is predicted along the 6-in. length parallel to the leading edge on elements. Failure is not predicted on element 8711, which is about 4 in. from the coil. This calculation appears to agree with the measurement in Fig. 24. However, at element 8326, which is 6 in. from the coil, stress exceeded the critical for failure that does not agree with measurement. However, there appears to be an instability in the analysis that makes this calculated result questionable.

Conclusions and Recommendations for Future Work

A method is presented in which the calculated impulsive force from an EIDI coil can be calculated and ice-airfoil skin can be modeled in an approximate manner using finite elements for dynamic analysis.

Agreement between calculated and measured transient displacements of the airfoil surface are reasonable. Overall, the most accurate results are obtained with a specified damping of 5%. Peak calculated displacements are within 0.005 in. of measured values.

The EIDI coil is located on the underside of the airfoil. Along the chord length, measured deflections are initially inward on the top side of the airfoil. Calculated results agreed with this measured trend.

Calculated interface shear stresses between the ice and airfoil skin are very high near the coil and decrease rapidly from the location of the impulse. In the chord direction, the decrease is the most rapid. At the location where the calculated shear stresses in the chord direction decrease below 50 psi, observed ice shedding ends.

Stability of the finite element model is a problem after about 1–1.5 ms. Changes in some of the parameters of the model may increase the length of time for stable calculations.

References

[1]Zumwalt, G. W., and Friedberg, R. A., "Designing an Electro-Impulse De-Icing System," AIAA Paper 86-0545, Jan. 1986.

[2]Schrag, R. L., and Zumwalt, G. W., "Electro-Impulse Deicing: Concept and Electrodynamic Studies," AIAA Paper 84-0021, Jan. 1984.

[3]Zumwalt, G. W., Schrag, R. L., Bernhart, W. D., and Friedberg, R. A., "Analysis and Tests for Design of an Electro-Impulse De-Icing Systems," NASA Rept. 174919, May 1985.

[4]Khatkhate, A. A., Scavuzzo, R. J. and Chu, M.L., "A Finite Element Study of the EIDI System," AIAA Paper 88-0022, Jan. 1988.

[5]Smythe, W. R., *Static and Dynamic Electricity,* McGraw-Hill, New York, 1950, pp. 290, 291.